MSW MANAGEMENT -Multidisciplinary, Scientific Work and Management Journal
ISSN: 1053-7899
Vol. 36 Issue 1, 2026, Pages: 1880-1891

Green-mediated synthesis of Ag–Ni bimetallic nanoparticles using *Mimosa pudica* leaf extract and their electrochemical performance

Dhanalakshmi Harichandran [a,b], Dhivya Paul[c*], Meiyazhagan Selvakumar [d]
[a] Research scholar, Nirmala College for women, Coimbatore - 641018
[b] Department of Science and Humanities, Karpagam College of Engineering, Coimbatore – 641032
[c] Department of Chemistry, Nirmala College for women, Coimbatore – 641018
[d] Department of Science and Humanities, Karpagam College of Engineering, Coimbatore - 641032
*Corresponding Author: Dr. P. Dhivya, E-mail: dhivsanto@gmail.com

Abstract: The development of sustainable and carbon-free electrode materials is critical for advancing next-generation electrochemical energy storage systems. In this work, Ag–Ni bimetallic nanoparticles (MPL-Ag@Ni BMNPs) were synthesized via a green, plant-mediated route using *Mimosa pudica* leaf extract as a natural reducing and stabilizing agent. The phytochemical constituents present in the extract facilitated the effective co-reduction of Ag and Ni ions under mild reaction conditions, eliminating the need for toxic chemical reagents. Comprehensive characterization using UV–visible spectroscopy, Fourier-transform infrared spectroscopy (FTIR), X-ray diffraction (XRD), field-emission scanning electron microscopy (FE-SEM), and energy-dispersive X-ray spectroscopy (EDX) confirmed the successful formation of bimetallic nanoparticles. XRD analysis revealed a face-cantered cubic crystal structure with an average crystallite size of approximately 11.5 nm, while FE-SEM images showed quasi-spherical nanoparticles with moderate aggregation and a porous morphology. EDX analysis further confirmed near-stoichiometric incorporation and uniform distribution of Ag and Ni. The electrochemical performance of the MPL-Ag@Ni BMNPs was evaluated as a supercapacitor electrode in 3 M KOH electrolyte using cyclic voltammetry and galvanostatic charge–discharge techniques. The electrode delivered a specific capacitance of approximately 128 F g^{-1} at a current density of 2 A g^{-1}, retained about 60% of its capacitance at 10 A g^{-1}, and maintained ~73% capacitance retention with ~99% coulombic efficiency after 10,000 charge–discharge cycles. The charge storage behaviour arises from a synergistic combination of electric double-layer capacitance and Ni-cantered pseudocapacitive redox reactions, with Ag enhancing electrical conductivity and charge transfer kinetics. Overall, this study demonstrates a simple, low-cost, and environmentally benign approach for producing Ag–Ni bimetallic electrodes suitable for sustainable alkaline supercapacitor applications.

Keywords: Green synthesis, Ag–Ni bimetallic nanoparticles, Mimosa pudica leaf extract, Plant-mediated synthesis, Pseudocapacitance, Electrochemical energy storage, Carbon-free electrode materials

1. Introduction

Electrochemical energy storage technologies are central to meet the rapidly increasing demand for efficient, reliable, and sustainable power sources required for portable electronics, electric vehicles, and renewable energy integration. Among these technologies, supercapacitors have attracted considerable attention because of their high-power density, fast charge–discharge capability, and long cycle life compared with conventional batteries (1, 2). However, their relatively low energy density and the dependence on costly or environmentally unfriendly electrode materials remain key obstacles to widespread commercialization. Consequently, the development of electrode materials that combine high electrochemical performance, low cost, and environmental sustainability is a critical research priority.

Nanotechnology provides effective strategies to address these challenges by enabling control over material structure and functionality at the nanoscale. Nanomaterials with dimensions below 100 nm exhibit physicochemical properties distinct from their bulk counterparts due to quantum confinement effects and high surface-to-volume ratios, which can significantly enhance electrochemical activity, ion diffusion, and charge transport kinetics(3–5). These characteristics are particularly advantageous for supercapacitor electrodes, where surface-driven processes and rapid redox reactions dominate energy storage behavior. Nevertheless, many conventional synthesis techniques for nanomaterials—such as hydrothermal, solvothermal, chemical reduction, and vapor deposition methods—often require toxic chemicals, high energy consumption, and complex processing steps, raising concerns regarding environmental impact and scalability (4, 6).

In response to these limitations, green synthesis approaches have emerged as sustainable alternatives for nanoparticle fabrication. Green synthesis exploits biological resources, including plant extracts, microorganisms, and biopolymers, to enable nanoparticle formation under mild and environmentally benign conditions. In plant-mediated synthesis, phytochemicals such as polyphenols, flavonoids, alkaloids, terpenoids, proteins, and reducing sugars act simultaneously as reducing, capping, and stabilizing agents (6). This multifunctional role eliminates the need for hazardous reagents while promoting controlled nanoparticle growth and improved surface functionality. Compared with microbial synthesis routes, plant-based methods offer advantages such as simplicity, rapid reaction kinetics, ease of scale-up, and the absence of pathogenic risks, making them especially attractive for sustainable materials development.

Beyond synthesis methodology, the composition of electrode materials plays a decisive role in determining supercapacitor performance. In this context, bimetallic nanoparticles have received increasing attention because the integration of two metals can generate synergistic effects that exceed the performance of monometallic systems. These synergistic interactions may include enhanced electrical conductivity, modified electronic structure, improved redox reversibility, and an increased density of electrochemically active sites(7, 8). Such features are highly beneficial for supercapacitor electrodes, where both fast electron transport and reversible faradaic reactions are essential.

Among various bimetallic systems, silver–nickel (Ag–Ni) combinations are particularly promising for alkaline supercapacitors. Nickel-based materials are well established as pseudocapacitive electrodes, exhibiting reversible Ni^{2+}/Ni^{3+} redox transitions in alkaline electrolytes that contribute significantly to faradaic charge storage(9, 10). However, their relatively low intrinsic electrical conductivity can limit rate capability and cycling efficiency. Silver, on the other hand, possesses excellent electrical conductivity and chemical stability, and when incorporated into Ni-based systems, it can facilitate rapid electron transport, reduce internal resistance, and enhance charge transfer kinetics without introducing significant parasitic redox reactions. Several studies have demonstrated that Ag incorporation into Ni-based electrodes leads to improved electrochemical reversibility and superior rate performance, particularly at high current densities (10, 11).

Despite these advantages, many high-performance Ag–Ni electrode architectures reported to date rely on complex hierarchical nanostructures or carbonaceous supports such as graphene, carbon nanotubes, or carbon nanofibers to achieve enhanced conductivity and surface area(12). While these approaches can deliver impressive electrochemical metrics, they often increase synthesis complexity, material cost, and environmental burden. In contrast, green-synthesized, carbon-free Ag–Ni bimetallic nanoparticles remain relatively underexplored, particularly for sustainable supercapacitor applications(10)

Mimosa pudica is a widely distributed medicinal plant known for its rich phytochemical composition, including alkaloids (notably mimosine), flavonoids, tannins, saponins, phenolic acids, and proteins. These biomolecules possess strong reducing and metal-chelating capabilities, making *Mimosa pudica* leaf extract an effective medium for green nanoparticle synthesis (13). While previous studies have reported the green synthesis of monometallic Ag or Ni nanoparticles using various plant extracts including this plant. reports on *Mimosa pudica*-assisted synthesis of Ag–Ni bimetallic nanoparticles especially for electrochemical energy storage applications are scarce.

MSW MANAGEMENT -Multidisciplinary, Scientific Work and Management Journal
ISSN: 1053-7899
Vol. 36 Issue 1, 2026, Pages: 1880-1891

In this study, we report a facile and environmentally benign synthesis of Ag–Ni bimetallic nanoparticles using *Mimosa pudica* leaf extract as a natural reducing and stabilizing agent. The structural, morphological, and compositional characteristics of the synthesized MPL-Ag@Ni bimetallic nanoparticles are systematically investigated using UV–visible spectroscopy, Fourier-transform infrared spectroscopy, X-ray diffraction, field-emission scanning electron microscopy, and energy-dispersive X-ray spectroscopy. Furthermore, the electrochemical performance of the green-synthesized Ag–Ni nanoparticles is evaluated as a supercapacitor electrode material in alkaline electrolyte, with emphasis on specific capacitance, rate capability, and long-term cycling stability. This work demonstrates the potential of plant-derived bimetallic nanoparticles as low-cost, environmentally friendly, and carbon-free electrode materials for next-generation energy storage.

2. Materials and Methods

2.1 Chemicals and Reagents

Silver nitrate ($AgNO_3$, ≥99.9%) and nickel (II) nitrate hexahydrate ($Ni(NO_3)_2 \cdot 6H_2O$, ≥99.5%) were purchased from Precision Scientific Company and used without further purification. Sodium hydroxide (NaOH, analytical grade) was used as the precipitating agent. All aqueous solutions were prepared using double-distilled water (DDW) to avoid contamination from dissolved ionic or organic impurities. All glassware was thoroughly cleaned, rinsed with DDW, and dried prior to use.

2.2 Collection and Preparation of Mimosa pudica Leaf Material

Fresh leaves of *Mimosa pudica* L. were collected from natural habitats in Pollachi (Tamil Nadu, India) and Palakkad (Kerala, India). The plant material was harvested during early morning hours to preserve maximum phytochemical content. Collected leaves were washed thoroughly with tap water to remove surface dust, followed by repeated washing with DDW to eliminate residual impurities. The cleaned leaves were air-dried under shade at ambient temperature for approximately two weeks until a constant weight was achieved. The dried leaves were then pulverized into a fine powder using a clean mechanical grinder and stored in airtight glass containers at room temperature until further use.

2.3 Preparation of Aqueous Mimosa pudica Leaf Extract

The aqueous extract of *Mimosa pudica* leaves was prepared following a simple and reproducible green extraction protocol. Briefly, a measured quantity of the dried and finely powdered *Mimosa pudica* leaves (typically 10 g) was dispersed in 100 mL of double-distilled water (DDW) in a clean borosilicate beaker. The suspension was heated at 60 °C for 30 min under gentle stirring to facilitate the release of bioactive phytochemicals into the aqueous medium.

After extraction, the reaction mixture was allowed to cool naturally to room temperature and subsequently filtered through Whatman No. 1 filter paper to remove insoluble plant residues. The resulting filtration was a clear, dark-colored aqueous leaf extract, indicating the presence of soluble phytochemical constituents such as polyphenols, flavonoids, proteins, and other reducing agents. The prepared extract was stored at 4 °C and used within one week to minimize phytochemical degradation and ensure reproducibility. The stepwise procedure involved in the preparation of the *Mimosa pudica* leaf extract is schematically illustrated in **Figure 1.**

Figure 1. Schematic representation of the preparation of *Mimosa pudica* leaf extract for green synthesis

2.4 Green Synthesis of Ag–Ni Bimetallic Nanoparticles

Ag–Ni bimetallic nanoparticles were synthesized via a plant-mediated co-reduction route using *Mimosa pudica* leaf extract as both reducing and stabilizing agent. In a typical synthesis, 50 mL of freshly prepared leaf extract was placed in a beaker and magnetically stirred at room temperature. To this solution, 25 mL of 0.2 M $Ni(NO_3)_2 \cdot 6H_2O$ was added dropwise under continuous stirring, and the mixture was allowed to react for 1 h to ensure homogeneous complexation between Ni^{2+} ions and phytochemical constituents.

Subsequently, 25 mL of 0.1 M NaOH solution was added slowly dropwise to the reaction mixture under constant stirring to induce the formation of nickel hydroxide intermediates. The reaction was maintained under stirring for an additional 2 h. Following this step, 20 mL of 0.1 M $AgNO_3$ solution was added dropwise, and the reaction mixture was left undisturbed overnight at room temperature to allow complete reduction of Ag^+ ions and formation of Ag–Ni bimetallic nanoparticles. The resulting precipitate was separated by decantation and washed repeatedly with DDW (2–3 times) to remove unreacted ions and soluble impurities, followed by washing with ethanol twice to eliminate residual organic components. The purified product was dried in a hot air oven at 80 °C and gently ground into a fine powder using an agate mortar. To improve crystallinity and remove residual organic moieties, the dried powder was calcined in a muffle furnace at 400 °C for 4 h under ambient atmosphere, yielding the final MPL-Ag@Ni bimetallic nanoparticles. The overall green synthesis route and post-treatment steps involved in the fabrication of MPL-Ag@Ni bimetallic nanoparticles are schematically illustrated in **Figure 2**.

Figure 2. Schematic illustration of the green synthesis and post-treatment process for MPL-Ag@Ni bimetallic nanoparticles using *Mimosa pudica* leaf extract.

MSW MANAGEMENT -Multidisciplinary, Scientific Work and Management Journal
ISSN: 1053-7899
Vol. 36 Issue 1, 2026, Pages: 1880-1891

2.5 Structural and Morphological Characterization

The optical properties of the *Mimosa pudica* leaf extract and synthesized nanoparticles were examined using UV–visible spectroscopy in the wavelength range of 200–800 nm. Fourier-transform infrared (FTIR) spectroscopy was employed to identify functional groups involved in metal ion reduction and nanoparticle stabilization. Crystalline phase identification and structural analysis were performed using X-ray diffraction (XRD) with Cu Kα radiation (λ = 1.5406 Å) over a 2θ range of 20–80°. The average crystallite size was estimated using the Scherrer equation. Surface morphology and particle size distribution were analyzed using field-emission scanning electron microscopy (FE-SEM). Elemental composition and metal distribution were determined by energy-dispersive X-ray (EDX) spectroscopy coupled with FE-SEM.

2.6 Electrochemical Measurements

Electrochemical measurements were carried out using a standard three-electrode configuration with a potentiostat /galvanostat. The MPL-Ag@Ni bimetallic nanoparticles were used as the working electrode material, while a platinum wire and Ag/AgCl electrode served as the counter and reference electrodes, respectively. All electrochemical experiments were conducted in 3 M KOH aqueous electrolyte at room temperature. Cyclic voltammetry (CV) measurements were performed over a potential window of 0–0.6 V (vs. Ag/AgCl) at scan rates ranging from 5 to 100 mV s^{-1}. Galvanostatic charge–discharge (GCD) measurements were conducted at current densities between 2 and 10 A g^{-1} to evaluate specific capacitance and rate capability. Cycling stability was assessed over 10,000 charge–discharge cycles to determine long-term electrochemical durability

3. Results and Discussion

3.1 UV Sprectoscopy analaysis

UV–visible spectroscopy was employed as a primary and rapid technique to monitor the formation and optical characteristics of the green-synthesized Ag–Ni bimetallic nanoparticles. **Figure 3(a)** presents the UV–visible absorption spectrum of the *Mimosa pudica* leaf extract, while **Figure 3(b)** shows the corresponding spectrum of the synthesized MPL-Ag@Ni bimetallic nanoparticles recorded in the wavelength range of 200–800 nm. The UV–visible spectrum of the *Mimosa pudica* leaf extract exhibits characteristic absorption bands in the ultraviolet region, typically between 250 and 300 nm, which can be attributed to π–π* and n–π* electronic transitions associated with polyphenols, flavonoids, and other aromatic phytochemical constituents present in the extract (13). These phytochemicals are well known to function as reducing and stabilizing agents in plant-mediated nanoparticle synthesis, facilitating the conversion of metal ions into zero-valent or mixed-valent metallic species.Upon completion of the green synthesis reaction, the UV–visible spectrum of the MPL-Ag@Ni bimetallic nanoparticles displays distinct changes compared to that of the pristine leaf extract. A broad and intense absorption band centered around ~420–440 nm is observed, which is characteristic of the surface plasmon resonance (SPR) of silver nanoparticles (3). The appearance of this SPR band confirms the successful reduction of Ag^{+} ions and the formation of nanoscale silver domains within the bimetallic system. In contrast, nickel-based nanoparticles do not typically exhibit a strong SPR feature in the visible region due to their electronic structure; instead, Ni contributions are generally reflected through weak or overlapping d–d transitions and broad background absorption (14).

Notably, the SPR band of silver in the MPL-Ag@Ni system appears broadened and slightly shifted compared to that of monometallic Ag nanoparticles reported in the literature. This behavior can be attributed to several factors, including bimetallic coupling between Ag and Ni, particle size distribution, surface roughness, and interactions with phytochemical capping agents . In bimetallic Ag–Ni systems, electronic interactions between the two metals can alter the local dielectric environment around Ag domains, leading to plasmon damping and peak broadening. Such spectral features are commonly interpreted as evidence of successful bimetallic formation rather than a simple physical mixture of individual monometallic nanoparticles.(15, 16)

The absence of sharp, well-defined multiple SPR peaks further suggests a relatively homogeneous distribution of Ag within the Ni-containing matrix, consistent with effective co-reduction mediated by the *Mimosa pudica* leaf extract. Similar UV–visible spectral behavior has been reported for plant-mediated Ag–Ni bimetallic nanoparticles synthesized using various botanical extracts, where phytochemical-assisted reduction leads to intimate metal–metal interactions and stabilized bimetallic nanostructures(14) Overall, the UV–visible spectroscopic results provide clear optical evidence for the successful green synthesis of MPL-Ag@Ni bimetallic nanoparticles. The combined presence of phytochemical-related absorption features and a broadened Ag SPR band confirms the dual role of *Mimosa pudica* leaf extract as both a reducing and stabilizing agent, laying the foundation for the subsequent structural and electrochemical characterizations discussed in the following sections

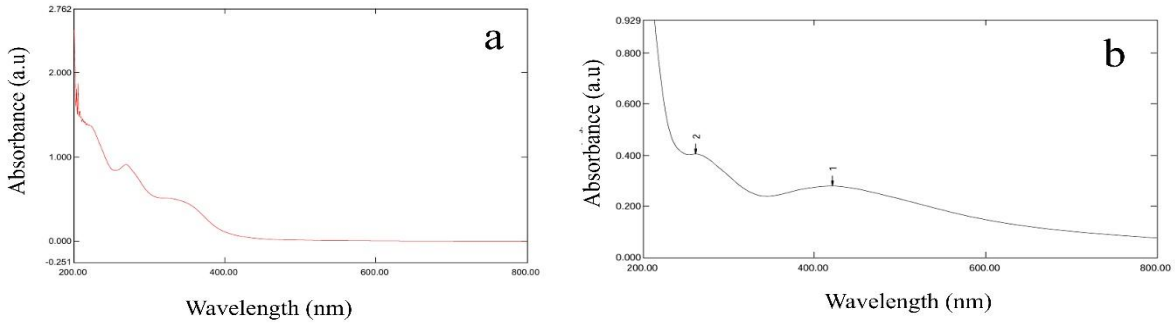

Figure 3 : (a) UV Spectra of Mimosa Pudica leaf Extract, (b) UV Spectra of Synthesised MPL-Ag@Ni BMNPs**.**

The synthesis of Ag–Ni bimetallic nanoparticles (Ag@Ni BMNPs) was accomplished with green approach, and characteristic absorption peaks at 261 and 421 nm were observed due to nickel-centered electronic transitions and surface plasmon resonance (SPR) of silver nanoparticles, respectively. The bands observed at 290 and 435 nm in the nanoparticle spectrum suggest the role of Salvia officinalis phytochemicals for reduction and stabilization of nanoparticles, which is also reported elsewhere (Majeed, Shahnaz, et al 2023). Similar plant-mediated steps of reduction involving Ag–Ni mono- and bimetallic nanoparticles were found elsewhere (Majid Rasool Kamli et al., 2022; Wojtaszek Konrad et al., 2023).

3.2 FTIR spectroscopy

Fourier-transform infrared (FTIR) spectroscopy was employed to identify the functional groups associated with the phytochemical constituents of *Mimosa pudica* leaf extract and to elucidate their role in the reduction, capping, and stabilization of the synthesized Ag–Ni bimetallic nanoparticles. Figure 4 shows the FTIR spectrum of the MPL-Ag@Ni bimetallic nanoparticles recorded in the range of 4000–500 cm^{-1}. The broad absorption bands observed in the high-wavenumber region at approximately 3600–3800 cm^{-1} are attributed to O–H

MSW MANAGEMENT -Multidisciplinary, Scientific Work and Management Journal
ISSN: 1053-7899
Vol. 36 Issue 1, 2026, Pages: 1880-1891

stretching vibrations of hydroxyl groups, which are characteristic of alcohols and phenolic compounds commonly present in plant extracts (13). These hydroxyl groups are widely reported to participate in the reduction of metal ions and in the stabilization of nanoparticles through hydrogen bonding and surface coordination. The presence of such broad O–H bands after nanoparticle formation indicates that phytochemical residues remain associated with the nanoparticle surface, acting as capping agents.

A weak to moderate band observed near 3050 cm^{-1} corresponds to aromatic C–H stretching vibrations, suggesting the presence of aromatic rings associated with flavonoids and polyphenolic compounds (17, 18). Additionally, the appearance of a low-intensity band around 2500–2600 cm^{-1} can be tentatively assigned to S–H stretching vibrations, indicating the possible involvement of sulfur-containing biomolecules in nanoparticle stabilization. While such assignments should be interpreted cautiously, similar features have been reported in plant-mediated nanoparticle systems and linked to thiol-containing proteins or secondary metabolites (13). The prominent absorption band centered around ~1600–1650 cm^{-1} is attributed to overlapping contributions from N–H bending vibrations of amide groups and C=C stretching vibrations of aromatic systems (19). This region is commonly associated with proteinaceous compounds and conjugated phytochemicals, suggesting that proteins or amino-acid-containing biomolecules from the leaf extract contribute to surface binding and stabilization of the bimetallic nanoparticles. The involvement of amide functionalities is further supported by bands observed in the region of 1350–1400 cm^{-1}, which can be assigned to C–N stretching vibrations of amines or amide III bands (13, 18). Additional bands in the range of 1200–1050 cm^{-1} are attributed to C–O stretching vibrations of alcohols, ethers, and phenolic groups, which are abundant in plant-derived polyphenols and carbohydrates [(17, 19)]. These functional groups are known to facilitate metal ion complexation and contribute to nanoparticle stabilization through coordination interactions. A weak band observed below 700 cm^{-1} may arise from out-of-plane bending vibrations of C–H groups or metal–oxygen related vibrations, although precise assignment in this region is often challenging due to overlapping lattice modes and residual organic contributions (18).

Overall, the FTIR results provide strong evidence that multiple functional groups present in the *Mimosa pudica* leaf extract including hydroxyl, amine, aromatic, and possibly thiol-containing groups play a cooperative role in the green synthesis of MPL-Ag@Ni bimetallic nanoparticles. These biomolecules act not only as reducing agents facilitating metal ion conversion but also as stabilizing ligands that prevent excessive particle agglomeration. The retention of phytochemical signatures in the FTIR spectrum of the final product confirms the successful plant-mediated fabrication of Ag–Ni bimetallic nanoparticles and supports their structural stability, which is beneficial for subsequent electrochemical applications.

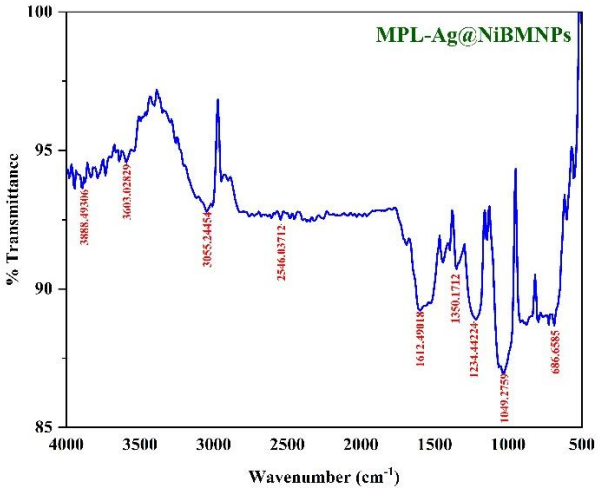

Figure 4. FT-IR spectrum of MPL-Ag@Ni bimetallic nanoparticles showing characteristic hydroxyl, amine, aromatic, and phenolic functional groups derived from *Mimosa pudica* leaf extract, confirming phytochemical-assisted reduction and stabilization during green synthesis.

3.3 X-Ray Crystallography Analaysis

X-ray diffraction (XRD) analysis was employed to investigate the crystalline structure, phase composition, and average crystallite size of the green-synthesized MPL-Ag@Ni bimetallic nanoparticles. The XRD pattern recorded in the 2θ range of 20–80° is presented in Figure 5. The diffraction pattern exhibits a series of well-defined peaks located at approximately 2θ ≈ 38.0°, 44.1°, 64.3°, and 77.2°, which can be indexed to the (111), (200), (220), and (311) crystallographic planes, respectively, characteristic of a face-centered cubic (fcc) structure. These reflections are consistent with standard diffraction data for metallic silver (JCPDS No. 04-0783) and nickel (JCPDS No. 04-0850), indicating the formation of crystalline metallic phases within the synthesized nanoparticles [(15, 20)]. Notably, the diffraction peak observed near 2θ ≈ 44.1° is relatively intense and broadened compared to the other reflections. This peak is commonly attributed to the overlapping contributions of the Ag (200) and Ni (111) planes, which occur at closely spaced diffraction angles in fcc Ag–Ni systems [(15)]. Such peak overlap is frequently reported in Ag–Ni bimetallic nanoparticles and suggests intimate structural association between the two metals rather than the presence of completely segregated monometallic phases. However, due to the similar lattice parameters of Ag and Ni and the inherent limitations of conventional XRD resolution, unequivocal distinction between alloyed and core–shell architectures cannot be made solely based on diffraction data.

The absence of additional impurity peaks corresponding to nickel oxides, silver oxides, or residual nitrate species indicates high phase purity of the synthesized MPL-Ag@Ni bimetallic nanoparticles. This observation confirms the effectiveness of the *Mimosa pudica*-assisted green synthesis route and subsequent thermal treatment in producing crystalline metallic nanoparticles without detectable secondary phases. The average crystallite size of the MPL-Ag@Ni bimetallic nanoparticles was estimated using the Scherrer equation applied to the most intense diffraction peak:

$$D = \frac{K\lambda}{\beta \cos\theta}$$

where D is the average crystallite size, K is the shape factor (taken as 0.9), λ is the X-ray wavelength (1.5406 Å for Cu Kα radiation), β is the full width at half maximum (FWHM) of the diffraction peak (in radians), and θ is the Bragg angle. Based on this analysis, the average crystallite size was determined to be approximately **11.5 nm**. The nanoscale crystallite size reflects effective nucleation control during plant-mediated synthesis and is advantageous for electrochemical applications due to the increased surface-to-volume ratio. Overall,

MSW MANAGEMENT -Multidisciplinary, Scientific Work and Management Journal
ISSN: 1053-7899
Vol. 36 Issue 1, 2026, Pages: 1880-1891

the XRD results confirm the successful formation of crystalline Ag–Ni bimetallic nanoparticles via the green synthesis route. The fcc crystal structure, absence of impurity phases, and nanoscale crystallite size collectively support the structural integrity of MPL-Ag@Ni nanoparticles and provide a solid basis for correlating structural features with the electrochemical behavior discussed in subsequent sections

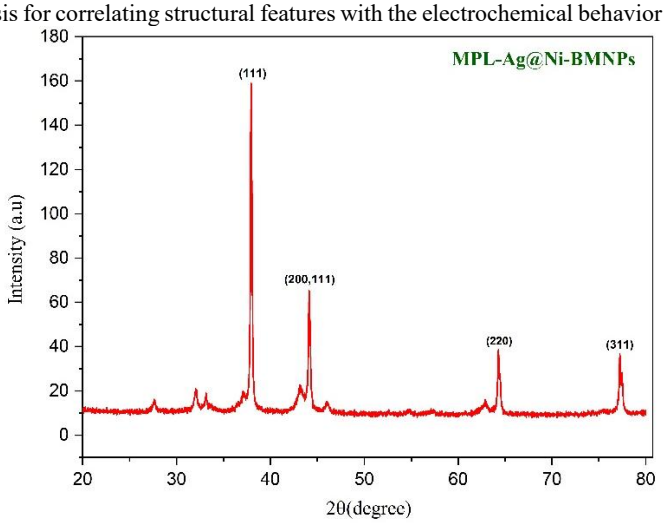

Figure 5 X-ray diffraction (XRD) pattern of green-synthesized MPL-Ag@Ni bimetallic nanoparticles

3.4 FE-SEM Analaysis

The FE-SEM images reveal that the synthesized MPL-Ag@Ni nanoparticles predominantly exhibit a quasi-spherical morphology with a relatively uniform particle distribution (**Figure 6**). The nanoparticles appear moderately aggregated, forming loosely packed clusters rather than dense agglomerates. Such aggregation is commonly observed in plant-mediated nanoparticle systems and is generally attributed to partial surface coverage by phytochemical capping agents, which can promote interparticle interactions while preventing complete particle coalescence. At higher magnification, the particle surfaces appear relatively smooth with no evidence of sharp faceting, suggesting isotropic growth during the reduction process. The observed morphology is consistent with nucleation and growth occurring under mild reaction conditions facilitated by phytochemicals present in the *Mimosa pudica* leaf extract. These biomolecules are known to regulate nanoparticle growth by coordinating metal ions and controlling reduction kinetics, thereby limiting excessive particle enlargement. The apparent particle size observed in FE-SEM images lies in the nanometer range and is in reasonable agreement with the average crystallite size (~11.5 nm) estimated from XRD analysis. Minor discrepancies between FE-SEM-observed particle dimensions and XRD-derived crystallite size are expected, as FE-SEM measures aggregated particle clusters, whereas XRD provides information on coherent crystalline domains within the particles. The presence of interparticle voids and a moderately porous arrangement is advantageous for electrochemical applications, as such morphology can facilitate electrolyte penetration and improve ion accessibility to electrochemically active sites.

Importantly, no distinct morphological separation between silver-rich and nickel-rich regions is evident from the FE-SEM images, suggesting intimate mixing of the two metallic components at the nanoscale. While FE-SEM alone cannot conclusively determine the internal architecture of the bimetallic nanoparticles, the uniform contrast and absence of phase-segregated domains support the formation of structurally integrated Ag–Ni nanoparticles. This observation is further corroborated by the elemental analysis discussed in the subsequent EDX section. Overall, the FE-SEM results confirm the successful formation of nanoscale Ag–Ni bimetallic particles with uniform morphology and moderate aggregation. The observed structural features—namely nanoscale dimensions, quasi-spherical shape, and porous agglomeration—are favorable for supercapacitor electrode applications, as they provide a balance between structural stability and electrochemically accessible surface area.

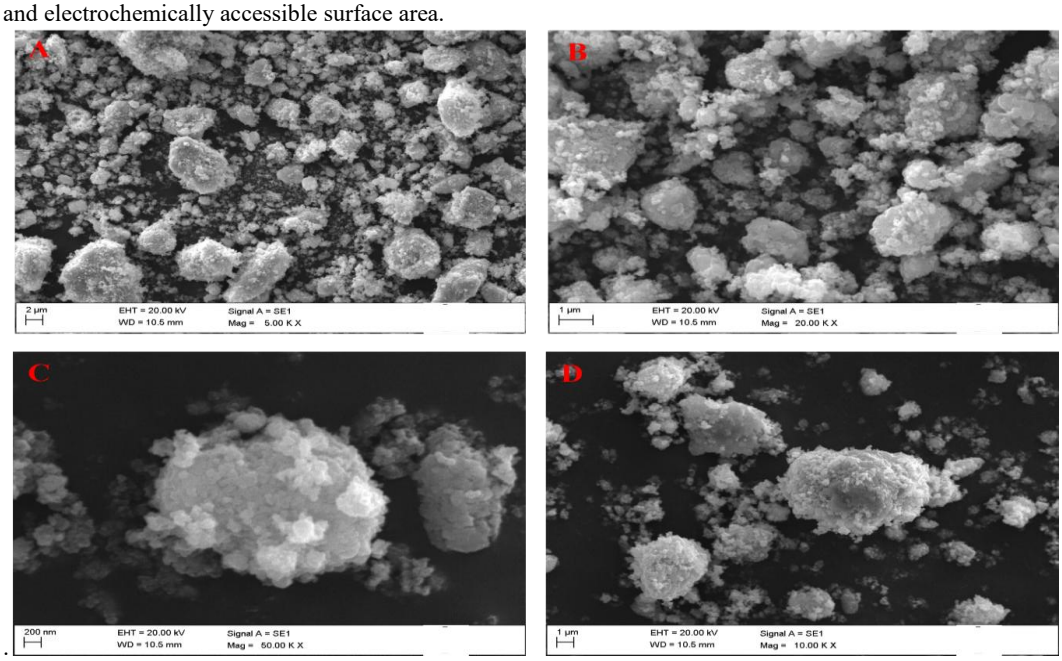

Figure 6 FE-SEM images of MPL-Ag@Ni bimetallic nanoparticles at different magnifications.

MSW MANAGEMENT -Multidisciplinary, Scientific Work and Management Journal
ISSN: 1053-7899
Vol. 36 Issue 1, 2026, Pages: 1880-1891

3.5 EDX Analaysis

As shown in **Figure 7**, EDX spectrum confirms the presence of silver (Ag) and nickel (Ni) as the dominant metallic constituents, with characteristic emission peaks observed at approximately 3.0–3.5 keV for Ag (Ag Lα) and 7.4–7.6 keV for Ni (Ni Kα), respectively. The absence of additional peaks associated with foreign metallic impurities indicates high compositional purity of the synthesized bimetallic nanoparticles. This observation corroborates the XRD results, which showed no detectable secondary phases or oxide impurities. Quantitative EDX analysis reveals that Ag and Ni are present in comparable proportions, with Ag accounting for approximately 44 wt% and Ni approximately 52 wt% of the total elemental composition. Minor contributions from carbon (~0.8 wt%) and nitrogen (~2.3 wt%) are also detected. These low-intensity signals are attributed to residual organic species originating from phytochemical capping agents present in the *Mimosa pudica* leaf extract and/or surface-adsorbed species remaining after thermal treatment. Similar observations have been widely reported for plant-mediated nanoparticle systems, where trace amounts of organic elements persist even after calcination and contribute to nanoparticle stabilization rather than structural impurity (15, 20, 21).

The near-stoichiometric Ag:Ni ratio observed in the present study suggests efficient co-reduction and homogeneous incorporation of both metals during the green synthesis process. In contrast, several earlier reports on Ag–Ni bimetallic nanoparticles have shown Ag-rich or Ni-rich compositions, depending on precursor concentration, reduction kinetics, and synthesis route (20). The balanced metal composition achieved here highlights the effectiveness of *Mimosa pudica* phytochemicals in regulating metal ion reduction and nucleation processes, thereby promoting uniform bimetallic formation. While EDX analysis provides reliable information on elemental composition, it is important to note that it does not offer definitive insight into the internal atomic arrangement (e.g., alloy versus core–shell structure). Nevertheless, the combined evidence from EDX, XRD, and FE-SEM analyses supports the formation of structurally integrated Ag–Ni bimetallic nanoparticles rather than a physical mixture of isolated monometallic particles.

Overall, the EDX results confirm the successful synthesis of compositionally uniform MPL-Ag@Ni bimetallic nanoparticles with minimal residual organic content. The homogeneous distribution of Ag and Ni is expected to play a crucial role in facilitating synergistic electrochemical behavior, where Ag enhances electrical conductivity and Ni contributes redox-active sites for charge storage, as discussed in the subsequent electrochemical performance section.

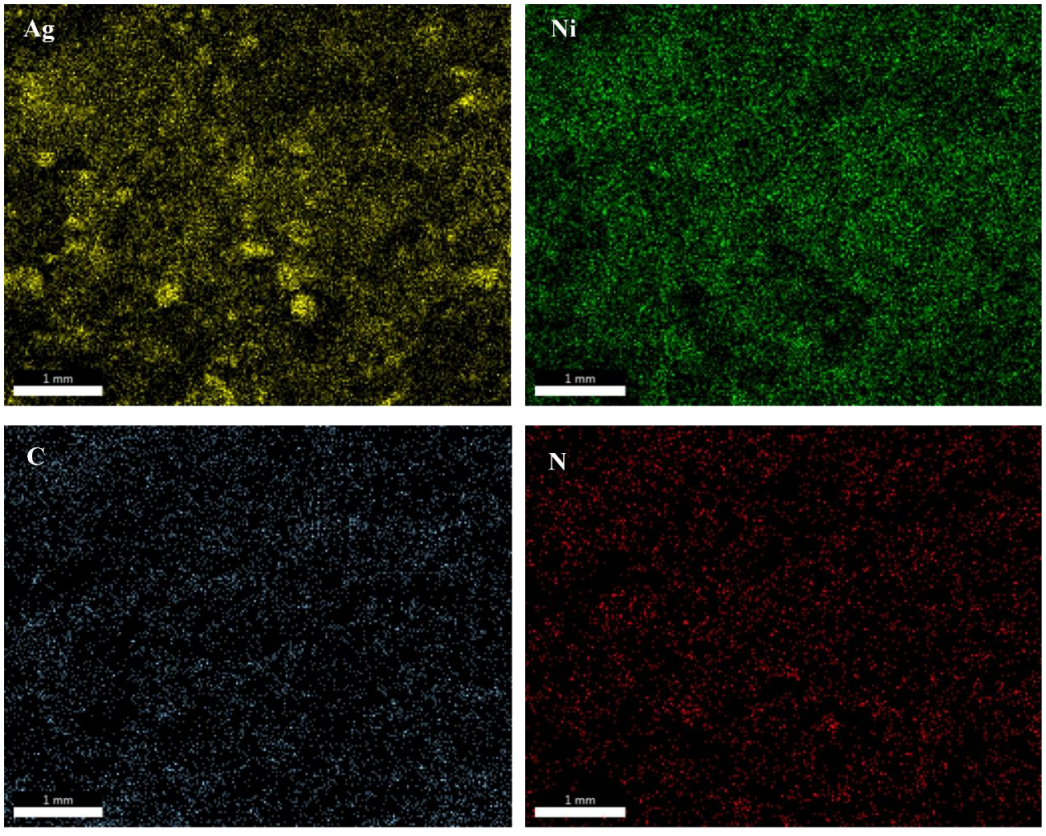

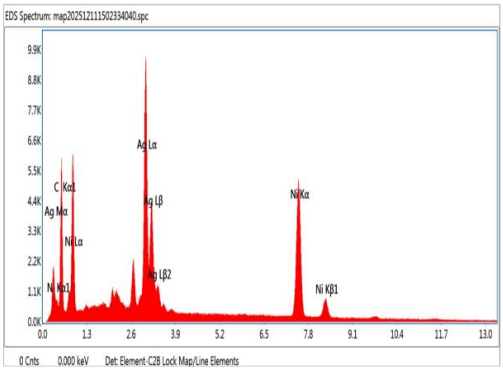

Element	Weight %	Atomic %
C	0.8	4.6
N	2.3	10.5
Ag	44.4	26.8
Ni	52.5	58.2

Figure 7 Energy-dispersive X-ray (EDX) elemental mapping and compositional analysis of green-synthesized MPL-Ag@Ni bimetallic nanoparticles. Elemental maps corresponding to Ag , Ni , C and N.

MSW MANAGEMENT -Multidisciplinary, Scientific Work and Management Journal
ISSN: 1053-7899
Vol. 36 Issue 1, 2026, Pages: 1880-1891

4. Electrochemical Behavior of MPL-Ag@Ni Bimetallic Nanoparticles

4.1 Cyclic Voltammetry Analysis

Cyclic voltammetry measurements were carried out within a potential window of 0–0.6 V (vs. Hg/HgO) at different scan rates ranging from 5 to 100 mV s^{-1}, as shown in **Figure 8**. All the CV curves exhibit quasi-rectangular profiles accompanied by broad anodic and cathodic peaks, indicating pseudocapacitance (Faradaic redox reaction) nature of the prepared electrode materials in 6 M KOH electrolyte. This redox feature is characteristic of reversible surface redox reactions associated with nickel species, typically attributed to the Ni^{2+}/Ni^{3+} transition occurring in alkaline electrolytes(10). The redox process can be represented by the following reaction:

$$Ni(OH)_2 + OH^- \leftrightarrow NiOOH + H_2O + e^-$$

The gradual increase in enclosed CV area and peak current with increasing scan rate from 5 to 100 mV s^{-1} demonstrates good electrochemical reversibility and fast charge propagation within the electrode material. Importantly, the overall CV shape is well retained even at higher scan rates, suggesting that the MPL-Ag@Ni electrode possesses favorable ion transport kinetics and structural stability under rapid polarization conditions. This behavior is essential for high-power supercapacitor applications. Silver does not exhibit prominent faradaic redox activity within the applied potential window. However, its incorporation plays a critical role in enhancing the overall electrochemical response. Owing to its high electrical conductivity, Ag facilitates efficient electron transport throughout the electrode matrix, thereby reducing internal resistance and improving charge transfer kinetics at the electrode–electrolyte interface (9, 10). This enhancement enables more effective utilization of Ni-based redox-active sites, particularly at higher scan rates where electronic limitations often dominate.

The peak currents associated with the redox features increase linearly with scan rate, indicating that the charge storage process is governed by a combination of surface-controlled pseudocapacitive reactions and diffusion-assisted processes. Such mixed charge-storage behavior has been widely reported for Ag–Ni bimetallic and hybrid systems and is considered advantageous, as it balances high capacitance with good rate capability

Compared to monometallic Ni-based electrodes, the MPL-Ag@Ni bimetallic nanoparticles exhibit better CV response and improved retention of capacitive features at elevated scan rates. This improvement can be attributed to the synergistic interaction between Ni-Ag, which provides redox-active centers making the system as an efficient electron-transport promoter. Similar synergistic effects have been reported for Ag-decorated $Ni(OH)_2$ nanosheets and Ag–Ni hybrid architectures, where Ag incorporation significantly improves electrochemical reversibility and power performance (11, 22). The CV results demonstrate that the green-synthesized MPL-Ag@Ni bimetallic nanoparticles exhibit a stable and reversible electrochemical response dominated by Ni-centered pseudocapacitance, with Ag enhancing electrical conductivity and charge transfer efficiency. These features highlight the suitability of MPL-Ag@Ni nanoparticles as promising electrode materials for supercapacitor applications(23).

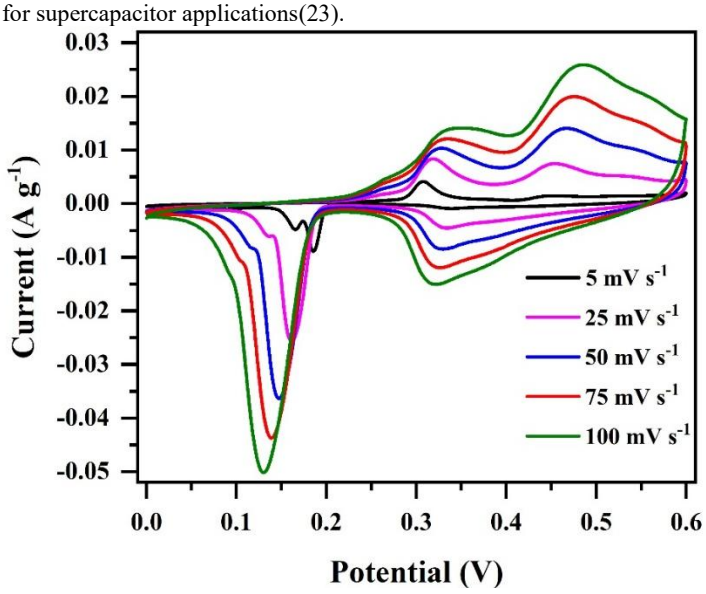

Figure 8. Cyclic voltammetry (CV) curves of Ag/Ni bimetallic nanoparticles

4.2 Galvanostatic Charge–Discharge and Capacitance Calculation

Galvanostatic charge–discharge (GCD) profiles were recorded in 6 M KOH electrolyte within a potential window of 0–0.6 V (vs. Hg/HgO) at current densities ranging from 2 to 10 A g^{-1}, as shown in **Figure 9**. The charge–discharge curves exhibit nearly symmetric non-triangular shapes with a slight curvature, indicating pseudocapacitive contributions of MPL-Ag@Ni electrode. The small voltage drop was observed at the beginning of the discharge process (IR drop) is minimal across all current densities, suggesting low internal resistance and efficient transport within the electrode. This behavior is consistent with the enhanced electrical conductivity provided by the Ag component in the bimetallic system, which facilitates rapid electron transfer during high-rate operation. The specific capacitance (C_{sp}) of the MPL-Ag@Ni electrode was calculated from the discharge curves using the standard equation:

$$C_{sp} = \frac{I \times \Delta t}{m \times \Delta V} \text{ F } g^{-1}$$

where I is the applied discharge current density, Δt is the discharge time, m is the mass of the active material, and ΔV is the potential window. Based on this analysis, the electrode delivers a high specific capacitance of 128 F g^{-1} at 2 A g^{-1}, which gradually decreases to about 88 F g^{-1} at 10 A g^{-1}. The decrease in specific capacitance with increasing current density can be attributed to kinetic limitations associated with ion diffusion and incomplete utilization of electrochemically active sites at higher charge–discharge rates. At low current densities, electrolyte ions have sufficient time to penetrate the porous nanoparticle network and access Ni-based redox sites, resulting in higher capacitance. In contrast, at higher current densities, only surface-accessible sites contribute effectively to charge storage, leading to reduced capacitance values. This trend is commonly observed in nanoparticle-based and pseudocapacitive electrode materials(10)

MSW MANAGEMENT -Multidisciplinary, Scientific Work and Management Journal
ISSN: 1053-7899
Vol. 36 Issue 1, 2026, Pages: 1880-1891

Importantly, the GCD profiles maintain their quasi-linear and symmetric characteristics across the entire range of current densities, indicating good coulombic efficiency and electrochemical reversibility. The absence of pronounced voltage plateaus further supports a pseudocapacitive charge storage mechanism dominated by fast surface redox reactions rather than battery-type intercalation processes. This observation aligns well with the CV results discussed in Section 4.1, confirming the pseudocapacitive nature of the MPL-Ag@Ni bimetallic electrode. Compared with previously reported green-synthesized Ni–Ag systems and carbon-free bimetallic electrodes, the specific capacitance achieved in this study is favorable, particularly considering the absence of hierarchical nanostructuring or conductive carbon supports. The results demonstrate that effective bimetallic synergy and optimized green synthesis can yield better electrochemical performance even in relatively simple nanoparticle architectures. Thus, the GCD analysis confirms that the MPL-Ag@Ni bimetallic nanoparticles exhibit high specific capacitance, good rate tolerance, and low internal resistance, highlighting their potential as sustainable electrode materials for supercapacitor applications.(9)

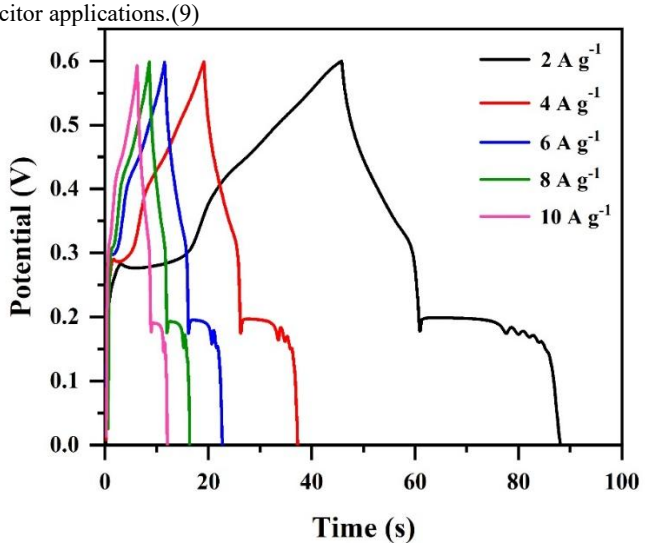

Figure 9. Galvanostatic charge–discharge (GCD) curves of Ag/Ni bimetallic electrode

4.3 Rate Capability

Figure 10 illustrates the variation of specific capacitance as a function of applied current density, derived from the galvanostatic charge–discharge measurements. The MPL-Ag@Ni electrode exhibits a gradual decrease in specific capacitance with increasing current density, retaining approximately 68.75% of its initial capacitance when the current density is increased from 2 to 10 A g^{-1}. Such behavior is characteristic of pseudocapacitive electrode materials, where both surface-controlled redox reactions and diffusion-assisted processes contribute to charge storage.

Importantly, the relatively high capacitance retention observed at elevated current densities highlights the favorable charge transport properties of the MPL-Ag@Ni bimetallic system. The incorporation of Ag plays a crucial role in this regard by providing highly conductive pathways that facilitate rapid electron transport and minimize polarization losses during high-rate operation. This enhancement enables more efficient utilization of Ni-centered redox-active sites even under fast charge–discharge conditions.

The moderate performance decay with increasing current density also reflects the nanoscale morphology and porous aggregation observed in FE-SEM analysis. The loosely packed nanoparticle clusters allow partial electrolyte penetration, which supports ion transport while maintaining structural integrity. Compared with previously reported carbon-free Ni-based and Ag–Ni hybrid electrodes, the rate capability achieved in this study is favorable, particularly considering the simplicity of the green synthesis route and the absence of conductive additives or hierarchical architectures(2, 10, 24, 25). The rate capability analysis confirms that the MPL-Ag@Ni bimetallic nanoparticles maintain stable capacitive performance over a wide range of current densities. This behavior emphasizes the synergistic interaction between Ag and Ni components and demonstrates the suitability of the green-synthesized MPL-Ag@Ni system for high-power supercapacitor applications.(7, 26)

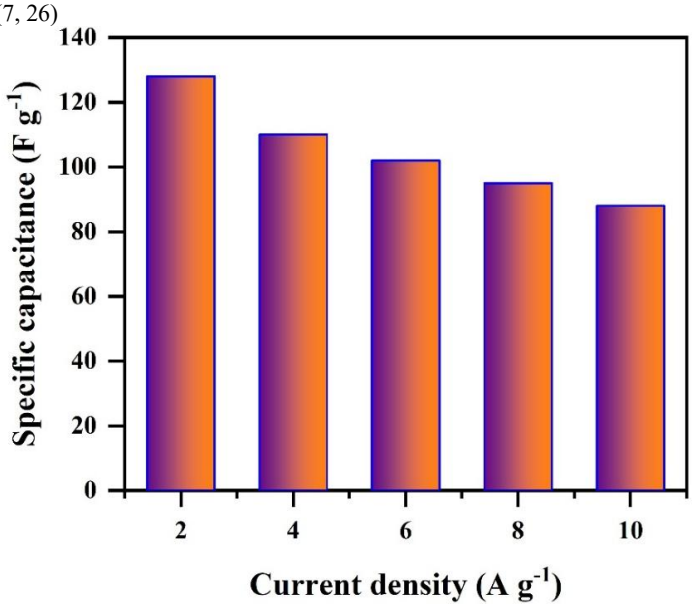

Figure 10. specific capacitance values as a function of current density.

MSW MANAGEMENT -Multidisciplinary, Scientific Work and Management Journal
ISSN: 1053-7899
Vol. 36 Issue 1, 2026, Pages: 1880-1891

4.4 Electrochemical Impedance Spectroscopy (EIS)

EIS was employed to elucidate the charge transport behavior and interfacial stability of the MPL-Ag@Ni bimetallic nanoparticle electrode before and after long-term cycling. **Figure 11** presents the Nyquist plots recorded in the frequency range of 0.01 Hz to 100 kHz, along with the corresponding equivalent circuit used to fit the experimental data. The impedance spectra consist of a small high-frequency intercept, a depressed semicircle in the high-to-medium frequency region, and a nearly vertical line in the low-frequency region, which is characteristic of pseudocapacitive electrode materials (9, 26).

The impedance response was fitted using an equivalent circuit comprising an inductive element (L1), a series resistance (R1), a parallel combination of charge-transfer resistance (R2) and a constant phase element (CPE1), followed by an additional constant phase element (CPE2). The inclusion of the inductive component (L1) accounts for the high-frequency inductive behavior arising from wiring, current collectors, and instrumental effects, which is commonly observed in electrochemical cells and does not influence the intrinsic electrochemical performance of the electrode.

The series resistance (R1) corresponds to the combined contribution of electrolyte resistance, intrinsic electrode resistance, and contact resistance between the active material and the current collector. The R1 value shows only a slight increase after 10,000 charge–discharge cycles, indicating stable electrode–electrolyte contact and minimal degradation of the electrolyte or current collector interface during prolonged cycling.(26, 27)

The depressed semicircle observed in the high-to-medium frequency region is represented by the parallel R2–CPE1 element. Here, R2 denotes the charge-transfer resistance associated with the Faradaic redox reactions of nickel species (Ni^{2+}/Ni^{3+}) at the electrode–electrolyte interface. The modest increase in R2 after extended cycling suggests minor interfacial polarization while confirming the preservation of efficient charge-transfer pathways. The use of CPE1 instead of an ideal capacitor reflects the non-ideal capacitive behavior arising from surface roughness, nanoparticle aggregation, and heterogeneity in the green-synthesized bimetallic electrode. In the low-frequency region, the impedance spectra exhibit a nearly vertical line with a slope close to 90°, indicating dominant capacitive behavior and efficient ion diffusion within the porous electrode structure. This response is modeled using a second constant phase element (CPE2), which represents distributed capacitance and ion transport within the porous nanoparticle network. The retention of this capacitive feature after 10,000 cycles confirms that the electrode maintains structural integrity and electrolyte accessibility during long-term operation.(28, 29)

Thus, this study substantiates that minimal changes in resistance components and the preservation of capacitive behavior after prolonged cycling highlight the electrochemical robustness of the MPL-Ag@Ni electrode. The Ag component effectively enhances electrical conductivity and stabilizes the electrode interface, while Ni provides reversible redox-active sites for pseudocapacitive charge storage. These EIS results are fully consistent with the excellent cycling stability and rate performance observed in the galvanostatic charge–discharge measurements, confirming the suitability of the green-synthesized MPL-Ag@Ni bimetallic nanoparticles for long-term supercapacitor applications

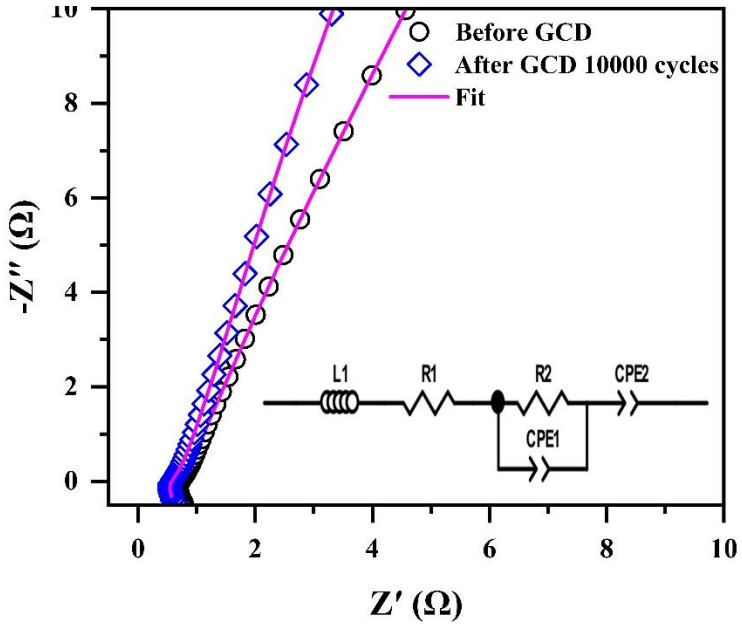

Figure 11 cycling performance of the MPL-Ag@Ni bimetallic nanoparticle

4.5 Cycling Stability and Coulombic Efficiency

The long-term electrochemical stability of the MPL-Ag@Ni bimetallic nanoparticle electrode was evaluated by continuous galvanostatic charge–discharge cycling at a fixed current density of 5 A g^{-1} over 10,000 cycles, as shown in **Figure 12**. Cycling stability is a critical performance metric for practical supercapacitor applications, as it reflects the structural robustness of the electrode material and the reversibility of the charge storage mechanism under prolonged operation.

As evident from **Figure 12**, the MPL-Ag@Ni electrode exhibits stable cycling behavior with a gradual and continuous decrease in capacitance, retaining approximately 73.11% of its initial capacitance after 10,000 cycles. This progressive decay, rather than an abrupt loss, suggests that the electrode does not suffer from catastrophic degradation such as severe delamination or structural collapse. Instead, the capacitance fading can be attributed to the long-term evolution of Ni-centered pseudocapacitive sites during repeated Ni^{2+}/Ni^{3+} redox transitions, which may lead to partial passivation or reduced accessibility of some electrochemically active sites over extended cycling. Such behavior is commonly observed in Ni-based pseudocapacitive electrodes operated in alkaline electrolytes and is considered acceptable for long-life supercapacitor operation.(26, 27)

In contrast to the gradual capacitance decay, the coulombic efficiency remains consistently high at approximately 98.65% throughout the entire cycling test, indicating highly reversible charge–discharge behavior. The coulombic efficiency (η) was calculated using the relation.

$$\eta = \frac{t_d}{t_c} \times 100\%$$

MSW MANAGEMENT -Multidisciplinary, Scientific Work and Management Journal
ISSN: 1053-7899
Vol. 36 Issue 1, 2026, Pages: 1880-1891

where t_d and t_c represent the discharge and charge times, respectively. The near-constant coulombic efficiency confirms that parasitic side reactions, electrolyte decomposition, and irreversible faradaic losses are minimal during long-term operation. This observation indicates that the dominant Ni-based pseudocapacitive redox reactions remain highly reversible in the Ag-enhanced bimetallic system.

The inset GCD profiles corresponding to the first 10 cycles and the last 10 cycles further support this conclusion. The preservation of similar charge–discharge curve shapes after prolonged cycling demonstrates sustained pseudocapacitive behavior, while the modest reduction in discharge time is consistent with the observed capacitance retention trend. Importantly, the symmetry of the GCD curves is maintained, corroborating the high coulombic efficiency and stable electrochemical reversibility.

The favorable cycling performance of the MPL-Ag@Ni electrode can be attributed to the synergistic effects of the bimetallic architecture. Nickel provides the primary redox-active centers for pseudocapacitive charge storage, whereas silver enhances electrical conductivity and mitigates localized current density hotspots, which can otherwise accelerate degradation in purely Ni-based electrodes. Additionally, the nanoscale morphology and moderate aggregation observed in FE-SEM analysis likely contribute to mechanical stability by accommodating volume changes associated with repeated Ni^{2+}/Ni^{3+} redox transitions.(9, 29)

Results in **Figure 12** demonstrate that the green-synthesized MPL-Ag@Ni bimetallic nanoparticles deliver durable charge storage with high electrochemical reversibility, achieving ~73% capacitance retention and ~99% coulombic efficiency after 10,000 cycles. These findings highlight the suitability of the MPL-Ag@Ni system as a carbon-free, sustainable electrode material for long-life supercapacitor applications, complementing its favorable rate capability and pseudocapacitive performance.

.

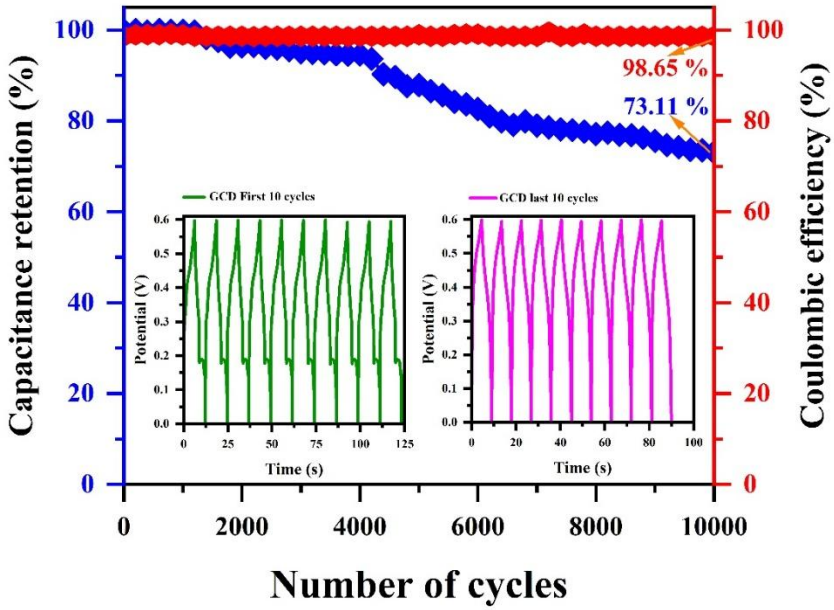

Figure 12 Long-term galvanostatic charge–discharge (GCD) cycling performance of the MPL-Ag@Ni bimetallic nanoparticle electrode measured at a current density of 5 A g^{-1} over 10,000 cycles. The plot shows capacitance retention (left axis) and coulombic efficiency (right axis) as a function of cycle number.

4.6 Comparison with Previously Reported Ag–Ni and Ni-Based Electrodes

For comparative evaluation of the electrochemical performance of the green-synthesized MPL-Ag@Ni bimetallic nanoparticles, previously reported Ag–Ni and Ni-based carbon-free supercapacitor electrodes are summarized in Table 1. The comparison highlights differences in specific capacitance, cycling durability, electrode architecture, and testing conditions reported in the literature. As shown in **Table 1**, several Ag–Ni or Ni-based electrodes exhibit higher specific capacitance values than the present MPL-Ag@Ni system; however, these performances are often achieved using complex architectures, such as hierarchical nanostructures, conductive polymer coatings, metal–organic frameworks, or carbonaceous supports. In contrast, the MPL-Ag@Ni electrode is synthesized via a simple plant-mediated green route, without the use of conductive carbon additives, polymer binders, or elaborate nanostructuring strategies. Despite this simplicity, the electrode delivers a competitive specific capacitance of 128 F g^{-1} at 2 A g^{-1} and demonstrates stable long-term cycling behavior.

Importantly, the MPL-Ag@Ni electrode maintains approximately 73% capacitance retention after 10,000 charge–discharge cycles, which is comparable to or exceeds the long-term stability reported for several Ag–Ni and Ni-based systems tested over fewer cycles. This highlights the structural robustness of the bimetallic nanoparticle architecture under prolonged electrochemical operation. The sustained coulombic efficiency (~99%) further confirms the high reversibility of the charge storage process, even as gradual capacitance fading occurs during extended cycling.

The balanced electrochemical performance of the MPL-Ag@Ni system can be attributed to the synergistic interaction between Ni-centered pseudocapacitive redox sites and Ag-induced enhancement of electrical conductivity. Nickel provides the primary Faradaic charge storage through reversible Ni^{2+}/Ni^{3+} redox transitions, while silver facilitates efficient electron transport and mitigates polarization effects, thereby improving electrochemical reversibility and cycling stability. Additionally, the nanoscale morphology and moderate aggregation of the green-synthesized nanoparticles likely contribute to mechanical integrity by accommodating volume changes associated with repeated redox cycling. This study demonstrates athat the MPL-Ag@Ni electrode does not aim to achieve record-high capacitance values, it offers a balanced combination of sustainability, simplicity, electrochemical durability, and carbon-free design. These attributes distinguish the present system from many previously reported Ag–Ni-based electrodes and underscore its potential as an environmentally benign and durable electrode material for practical supercapacitor applications.

MSW MANAGEMENT -Multidisciplinary, Scientific Work and Management Journal
ISSN: 1053-7899
Vol. 36 Issue 1, 2026, Pages: 1880-1891

Table 1 A comparative summary with related MPL-Ag@Ni bimetallic systems is shown below:

Electrode Materials	C*sp* (A g^{-1} or mV /s)	Cycling Stability (%)	References
$Ni(OH)_2$@Ag	945 @ 1 A g^{-1}	92% (1000 cycles)	(27)
$NiCo_2O_4$/NF@PPy	194 @ 30 A g^{-1}	89.5 % (10,000 cycles)	(26)
Ag/NiO composites	812 @5 Mv/s	89.2 % (5000 cycles)	(9)
Ag/NiO-MOF derived	1454 @1 A g^{-1}	3000 cycles	(30)
NiCoLDH	1800C/cm2	82.7% (20,000)	(31)
MPL-Ag@Ni	128 @ 2 A g^{-1}	~73% (10,000 cycles)	This Present Study

5. Conclusions

In this study, Ag–Ni bimetallic nanoparticles were successfully synthesized via a simple and sustainable green route using *Mimosa pudica* leaf extract as a natural reducing and stabilizing agent. Structural and morphological characterizations confirmed the formation of crystalline, nanoscale Ag–Ni particles with uniform elemental distribution and moderate aggregation. FT-IR analysis demonstrated the involvement of phytochemical functional groups in nanoparticle stabilization, while XRD and FE-SEM results confirmed high phase purity and a favorable nanoscale morphology.

Electrochemical investigations revealed that the MPL-Ag@Ni electrode exhibits pronounced pseudocapacitive behavior dominated by Ni-centered redox reactions, with Ag playing a key role in enhancing electrical conductivity and facilitating efficient charge transfer. The electrode delivered a specific capacitance of approximately 128 F g^{-1} at 2 A g^{-1}, demonstrated good rate capability, and maintained stable long-term electrochemical performance with ~73% capacitance retention and ~99% coulombic efficiency after 10,000 charge–discharge cycles. The gradual capacitance decay observed during extended cycling indicates progressive surface evolution rather than abrupt structural degradation, confirming sustained electrochemical reversibility.

Importantly, these electrochemical performances were achieved without the use of conductive carbon additives, polymer binders, or complex nano structuring strategies, highlighting the effectiveness of the bimetallic design and the green synthesis approach. Overall, this work demonstrates that plant-mediated Ag–Ni bimetallic nanoparticles offer a balanced combination of sustainability, electrochemical durability, and carbon-free design, making them promising electrode materials for environmentally benign supercapacitor applications.

Acknowledgement

The authors gratefully acknowledge Dr. A. Murugan, Assistant Professor, Department of Science and Humanities, Karpagam College of Engineering, Coimbatore, for his valuable support and guidance during the synthesis of the Ag–Ni bimetallic nanoparticles and for assistance with cyclic voltammetry applications. The authors also thank Ms. D. Sudha, Assistant Professor, Department of Science and Humanities, Karpagam College of Engineering, Coimbatore, for her support in procuring the required chemicals for this study. Special thanks are extended to Mr. Robin Antony Raj, Laboratory Technician, for his assistance with laboratory facilities and experimental support.

References

1. **Zhao J**, **Burke AF**. Review on supercapacitors: Technologies and performance evaluation. *Journal of Energy Chemistry* 59 Elsevier B.V.: 276–291, 2021.
2. **Rani L**, **Han JI**. Engineering MXene/nickel-silver sulfide composites for high-performance hybrid supercapacitors: Synthesis and electrochemical insights. *Chemical Engineering Journal* 522, 2025. doi: 10.1016/j.cej.2025.167423.
3. **Adekoya JA**, **Dare EO**, **Mesubi MA**, **Revaprasadu N**. Synthesis and Characterization of Optically Active Fractal Seed Mediated Silver Nickel Bimetallic Nanoparticles. *J Mater* 2014: 1–9, 2014. doi: 10.1155/2014/184216.
4. **Jamkhande PG**, **Ghule NW**, **Bamer AH**, **Kalaskar MG**. Metal nanoparticles synthesis: An overview on methods of preparation, advantages and disadvantages, and applications. *J. Drug Deliv. Sci. Technol.* 53 Editions de Sante: 2019.
5. **Zaleska-Medynska A**, **Marchelek M**, **Diak M**, **Grabowska E**. Noble metal-based bimetallic nanoparticles: The effect of the structure on the optical, catalytic and photocatalytic properties. *Adv Colloid Interface Sci* 229: 80–107, 2016. doi: 10.1016/j.cis.2015.12.008.
6. **Dhand C**, **Dwivedi N**, **Loh XJ**, **Jie Ying AN**, **Verma NK**, **Beuerman RW**, **Lakshminarayanan R**, **Ramakrishna S**. Methods and strategies for the synthesis of diverse nanoparticles and their applications: A comprehensive overview. *RSC Adv.* 5 Royal Society of Chemistry: 105003–105037, 2015.
7. **Aljamhi WA**, **Hammud HH**, **Parveen N**, **Ansari SA**, **Mazher J**, **Alameddine B**, **Baig N**, **Das N**, **Wahed SA**. Synergistic enhancement of capacitance and catalysis by cobalt binary ligand complexes on porous carbon and nano silica. .
8. **Murugadoss G**, **Venkatesh N**, **Kandhasamy N**, **Zaporotskova I**, **Govindarajan D**, **Kumaresan N**, **Kirubaharan K**, **Khanapuram UK**, **Kheawhom S**. Synergistic effects of metal-modified carbon nanotubes: experimental characterization and theoretical modeling for energy and environmental solutions. .
9. **Chinnaiah K**, **Kannan K**, **Krishnamoorthi R**, **Palko N**, **Gurushankar K**. Nanostructured Ag/NiO composites for supercapacitor and antibacterial applications, and in-silico theoretical investigation. *Journal of Physics and Chemistry of Solids* 184, 2024. doi: 10.1016/j.jpcs.2023.111730.
10. **Nagamuthu S**, **Ryu KS**. Synthesis of Ag/NiO Honeycomb Structured Nanoarrays as the Electrode Material for High Performance Asymmetric Supercapacitor Devices. *Sci Rep* 9, 2019. doi: 10.1038/s41598-019-41446-0.
11. **Cao J**, **Yun J**, **Zhang N**, **Wei Y**, **Yang H**, **Xu Z**. Bifunctional Ag@Ni-MOF for high performance supercapacitor and glucose sensor. *Synth Met* 282, 2021. doi: 10.1016/j.synthmet.2021.116931.
12. **Delel ZY**, **Worku AK**, **Alemu MA**, **Ayele DW**, **Yaseen ZM**. Engineering of Cu and Ag-doped reduced graphene oxide for supercapacitor electrode applications. *Journal of Physics and Chemistry of Solids* 208, 2026. doi: 10.1016/j.jpcs.2025.112999.
13. **Gopinath M**, **Bharathiraja B**, **Iyyappan J**, **Gnanasekaran R**, **Yuvaraj D**, **Dhithya V**. Extracellular Green Synthesis of Silver Nanoparticles Using Extract of Mimosa pudica Leaves and Assessment of Antibacterial and Antifungal Activity. *Proceedings of the National Academy of Sciences India Section B - Biological Sciences* 90: 1025–1033, 2020. doi: 10.1007/s40011-020-01175-1.

MSW MANAGEMENT -Multidisciplinary, Scientific Work and Management Journal
ISSN: 1053-7899
Vol. 36 Issue 1, 2026, Pages: 1880-1891

14. **Idris DS**, **Roy A**, **Malik A**, **Khan AA**, **Sharma K**, **Roy A**. Green Synthesis of Silver Oxide-Nickel Oxide Bimetallic Nanoparticles Using Peels of Citrus Sinensis and their Application. *J Inorg Organomet Polym Mater* 35: 594–606, 2025. doi: 10.1007/s10904-024-03316-9.
15. **Kamli MR**, **Alzahrani EA**, **Albukhari SM**, **Ahmad A**, **Sabir JSM**, **Malik MA**. Combination Effect of Novel Bimetallic Ag-Ni Nanoparticles with Fluconazole against Candida albicans. *Journal of Fungi* 8, 2022. doi: 10.3390/jof8070733.
16. **Wojtaszek K**, **Cebula F**, **Rutkowski B**, **Wytrwal M**, **Csapó E**, **Wojnicki M**. Synthesis and Catalytic Study of NiAg Bimetallic Core–Shell Nanoparticles. *Materials* 16, 2023. doi: 10.3390/ma16020659.
17. **Gupta RK**, **Kumar V**, **Gundampati RK**, **Malviya M**, **Hasan SH**, **Jagannadham M V.** Biosynthesis of silver nanoparticles from the novel strain of Streptomyces Sp. BHUMBU-80 with highly efficient electroanalytical detection of hydrogen peroxide and antibacterial activity. *J Environ Chem Eng* 5: 5624–5635, 2017. doi: 10.1016/j.jece.2017.09.029.
18. **Majeed S**, **Mohd Rozi NAB**, **Danish M**, **Mohamad Ibrahim MN**, **Joel EL**. Invitro apoptosis and molecular response of engineered green iron oxide nanoparticles with L-arginine in MD-MBA 231 breast cancer cells. *J Drug Deliv Sci Technol* 80, 2023. doi: 10.1016/j.jddst.2023.104185.
19. **Aarthi J**, **Kaviya SS**, **Kirubavathi K**, **Selvaraju K**, **Shakeel F**, **Gowri S**, **Faiyazuddin M**. Green synthesis of nickel oxide nanoparticles using leaf extract of Mimosa pudica for killing triple-negative breast cancer MDA-MB-231 cells and bacteria. *J Mol Struct* 1321, 2025. doi: 10.1016/j.molstruc.2024.140178.
20. **Egbewole BI**, **Ogunsile BO**, **Adeola AO**, **Olawade DB**, **Adekunle YA**, **Nomngongo PN**. Mallotus oppositifolius-mediated biosynthesis of bimetallic nanoparticles of silver and nickel: antimicrobial activity and plausible mechanism(s) of action. *Biomass Convers Biorefin* 14: 14083–14094, 2024. doi: 10.1007/s13399-022-03463-4.
21. **Yonan EN**, **Sher Mohammed NM**, **Qasim AK**. Green synthesis and characterisation of monometallic (Ni) and bimetallic (Ni-Ag) nanoparticles using Cicer Arietinum leaf extract and their applications for adsorption of toluidine blue. *Int J Environ Anal Chem* 104: 5264–5279, 2024. doi: 10.1080/03067319.2022.2118594.
22. **samea SG abdel**, **Omran MM**, **Aman D**, **Zaki EG**, **Mahmoud SB**. Development of carbonized paper-supported electrodes with covalent organic frameworks for next-generation sustainable supercapacitors. *Synth Met* 318: 118089, 2026. doi: 10.1016/j.synthmet.2026.118089.
23. **Augustyn V**, **Simon P**, **Dunn B**. Pseudocapacitive oxide materials for high-rate electrochemical energy storage. *Energy Environ. Sci.* 7 Royal Society of Chemistry: 1597–1614, 2014.
24. **Kavitha ER**, **Meiyazhagan S**, **Yugeswaran S**, **Balraju P**, **Suresh K**. Electrochemical prospects and potential of hausmannite Mn3O4 nanoparticles synthesized through microplasma discharge for supercapacitor applications. *Int J Energy Res* 45: 7038–7056, 2021. doi: 10.1002/er.6288.
25. **Kavitha ER**, **Meiyazhagan S**, **Yugeswaran S**, **Suresh K**. Expeditious and single step synthesis of ceria quantum dots by microplasma discharge method for supercapacitor applications. *Mater Chem Phys* 318, 2024. doi: 10.1016/j.matchemphys.2024.129319.
26. **BoopathiRaja R**, **Parthibavarman M**. Desert rose like heterostructure of NiCo2O4/NF@PPy composite has high stability and excellent electrochemical performance for asymmetric super capacitor application. *Electrochim Acta* 346, 2020. doi: 10.1016/j.electacta.2020.136270.
27. **Wang K**, **Zhang X**, **Zhang X**, **Chen D**, **Lin Q**. A novel Ni(OH)2/graphene nanosheets electrode with high capacitance and excellent cycling stability for pseudocapacitors. *J Power Sources* 333: 156–163, 2016. doi: 10.1016/j.jpowsour.2016.09.153.
28. **Zeng H-C**, **Qiu P-F**, **Huang Z**, **Tan X-N**, **Huang Z-Y**, **Zhou Y**. Controllable synthesis and morphology engineering of S-doped NiCo layered double hydroxide nanoflowers for high-performance supercapacitors. *J Power Sources* 665: 238966, 2026. doi: 10.1016/j.jpowsour.2025.238966.
29. **Chinnaiah K**, **Kannan K**, **Palko N**, **Grishina M**, **Guganathan L**, **Gurushankar K**. Bioengineered Ag/NiO nanocomposites as advanced battery-supercapacitor electrodes for highly efficient symmetric hybrid devices. *Ionics (Kiel)* 30: 1691–1707, 2024. doi: 10.1007/s11581-023-05361-9.
30. **Zhou LX**, **Yang YY**, **Zhu HL**, **Zheng YQ**. In situ synthesis of Ag/NiO derived from hetero-metallic MOF for supercapacitor application. *Chemical Papers* 75: 1795–1807, 2021. doi: 10.1007/s11696-020-01431-8.
31. **Wang X**, **Li X**, **Du X**, **Ma X**, **Hao X**, **Xue C**, **Zhu H**, **Li S**. Controllable Synthesis of NiCo LDH Nanosheets for Fabrication of High-Performance Supercapacitor Electrodes. *Electroanalysis* 29: 1286–1293, 2017. doi: 10.1002/elan.201600602.